

# Inverse Kinematics of Anthropomorphic Arms Yielding Eight Coinciding Circles

B. Bongardt<sup>1</sup>

<sup>1</sup>DFKI GmbH, Robotics Innovation Center, Robert-Hooke-Str. 1, 28359 Bremen, Germany, e-mail: bertold.bongardt@dfki.de

**Abstract.** In this paper it is demonstrated that the solution space of the inverse kinematic problem of an anthropomorphic, redundant 7R chain for a given pose does consist of eight different coinciding circles instead of a single circle that has been reported as of today. By modeling the structure using the convention by Sheth and Uicker, the displacements within the kinematics of the chain are partitioned in time-invariant displacements along rigid links and time-variant displacements along the seven rotative joints. In particular, the subchains of shoulder, elbow, and wrist are preserved. By respecting the ‘flips’ of these three substructures the eight-fold occupancy of the redundancy circle is obtained. The result corresponds to the eight IK solutions for regional-spherical arms and provides a prerequisite for using all capabilities of respective robots in practical applications.

**Key words:** Kinematic analysis, anthropomorphic robot arm, redundant manipulator, cyclic law of cosines, virtual joints.

## 1 Introduction

The inverse kinematic problem (IKP) of a redundant robot is seeking for an infinite set of joint configurations for a given orientation and position of its endeffector. Since robotic chains with seven degree of freedom (DOF) possess a kinematic redundancy of degree one in the six-dimensional space of poses  $SE(3)$  the solution space of the IKP of chains with seven rotative joints (7R) is characterized by one-dimensional manifolds: each containing  $\infty^1$  points representing certain joint configurations. Kinematic 7R chains with intersecting axes of the first and the last three joints (*shoulder* and *wrist*) are called anthropomorphic arms. Their structure can be grouped in two spherical submechanisms and one rotative (*elbow*) element and thus be called an  $SR\delta$  structure. The *self-motions* [5, 9] or *null-space motions* [7] – those joint configuration changes that let the endeffector’s pose remain constant – of an anthropomorphic 7R arm can be characterized by the *redundancy circle* [1, 6, 9]. The solution set for a given pose has been computed [12] as specific interval sets for the redundancy angle (circle segments for the elbow position) that depend on minimally and maximally feasible values of the seven joints.

The approach of this paper is based on the works by Shimizu et al. [12]: the robot redundancy is parametrized by the elbow angle with respect to redundancy circles. The modeling here employs the kinematic convention by Sheth and Uicker [11],

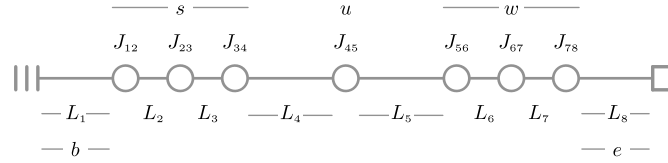


Fig. 1: Overview of used notation for links, joints, and joint groups of the 7R chain.

instead of the convention by Denavit and Hartenberg [8]. Due to the advantageous properties of this convention [4], the kinematic SRS structure of the robot is well reflected and the analytic solution procedure is simplified. As main contribution, the approach yields the insight that a complete solution of the inverse kinematics does not incorporate *one* but *eight* different one-parameter sets in parameter space which each represent eight circles coinciding in  $\mathbb{R}^3$ , the Euclidean workspace [2, 3].<sup>1</sup>

The structure of the paper reads as follows: In Sec. 2 the robot model is introduced and the forward kinematics is computed. Sec. 3 presents geometric analysis within three planes of the robot's geometry. Sec. 4 contains the computation of the inverse kinematics, including a brief example. The paper is concluded in Sec. 5.

## 2 Forward Kinematics

The eight links of the 7R chain are enumerated by a simple index from the index set  $\mathcal{I}_L = (1, 2, \dots, 8)$ . The seven joints are equipped with a double index from  $\mathcal{I}_J = ((1, 2), (2, 3), \dots, (7, 8))$ . The first and the last three joints are referred by  $s$  (shoulder) and by  $w$  (wrist). The elbow is denoted by  $u$  (cubital). The reference location at the first link is called  $b$  (basis) and the reference location of the last link is called  $e$  (endeffector), see the sketch in Figure 1.

The description of the geometry of an anthropomorphic arm (Mitsubishi PA10) is given in Table 1 in terms of its Sheth–Uicker parameters. The values  $b = 0$  in each row reflect that each sequential pair of joint axes is intersecting. The spherical constellation of the first three and last three joint axes is reflected by zeros of the translative parameters in the rows 2-3 and 6-7. The reference posture of the robot in Table 1 represents a fully-stretched configuration (as displayed in Figure 4a).

By means of the Sheth–Uicker specification, the forward kinematics of the 7DOF kinematic chain for a configuration vector  $\mathbf{q} = (q_{12}, q_{23}, q_{34}, q_{45}, q_{56}, q_{67}, q_{78})$ , with  $\mathbf{q} = \mathbf{q}^{(t)}$  for a certain time  $t$ , as the chain of matrix multiplications

$$\mathbf{D}_{be} = \text{FK}(\mathbf{q}) = \mathbf{L}_1 \cdot \mathbf{J}_{12} \cdot \mathbf{L}_2 \cdot \mathbf{J}_{23} \cdot \mathbf{L}_3 \cdot \mathbf{J}_{34} \cdot \mathbf{L}_4 \cdot \mathbf{J}_{45} \cdot \mathbf{L}_5 \cdot \mathbf{J}_{56} \cdot \mathbf{L}_6 \cdot \mathbf{J}_{67} \cdot \mathbf{L}_7 \cdot \mathbf{J}_{78} \cdot \mathbf{L}_8. \quad (1)$$

Each link displacement  $\mathbf{L}_k$  is given as a time-invariant displacement parametrized by a dual Euler angle  $(\tilde{\gamma}_k, \tilde{\beta}_k, \tilde{\alpha}_k)$  as  $\mathbf{L}_k = \mathbf{L}(\gamma_k, c_k, \beta_k, b_k, \alpha_k, a_k)$  for all  $k \in \mathcal{I}_L$  and each joint displacement  $\mathbf{J}_{ij} = \mathbf{J}(q_{ij}) = \mathbf{D}_z(q_{ij})$  is given as time-variant  $z$ -rotation for all  $(i, j) \in \mathcal{I}_J$  [2, 4].

<sup>1</sup> In terminology of [12], the complete solution reported here incorporates the inversion of the three cosine-type into the solution procedure. In comparison to the recent work [10] which employs a parametrization with respect to the second joint, the parametrization via the redundancy angle permits the direct interpretation as eight coinciding elbow circles.

Link	$q_{ij}$	$d_{ij}$	$\gamma_j$	$c_j$	$\beta_j$	$b_j$	$\alpha_j$	$a_j$
1	-	-	-	$l_{bs}/2$	-	-	-	$l_{bs}/2$
2	$q_{12}$	-	-	-	$-\pi/2$	-	-	-
3	$q_{23}$	-	-	-	$+\pi/2$	-	-	-
4	$q_{34}$	-	-	$l_{su}/2$	$-\pi/2$	-	-	$l_{su}/2$
5	$q_{45}$	-	-	$l_{uw}/2$	$+\pi/2$	-	-	$l_{uw}/2$
6	$q_{56}$	-	-	-	$-\pi/2$	-	-	-
7	$q_{67}$	-	-	-	$+\pi/2$	-	-	-
8	$q_{78}$	-	-	$l_{we}/2$	-	-	-	$l_{we}/2$

Table 1: Sheth–Uicker parameters of an anthropomorphic 7R arm with sequentially-orthogonal joint axes. The numerical lengths *base–shoulder*, *shoulder–elbow*, *elbow–wrist*, and *wrist–effector* are  $l_{bs} = 31.7$  cm,  $l_{su} = 38.0$  cm,  $l_{uw} = 48.0$  cm, and  $l_{we} = 12.28$  cm for the Mitsubishi PA10.

For the rotative part  $\mathbf{R}_{be} = \mathbf{E}_e$  of  $\mathbf{D}_{be} = \begin{pmatrix} \mathbf{R}_{be} & \mathbf{t}_{be} \\ \mathbf{0} & 1 \end{pmatrix} = \begin{pmatrix} \mathbf{P}_e & \mathbf{p}_e \\ \mathbf{0} & 1 \end{pmatrix} = \mathbf{P}_e$ , the forward kinematics of Equation 1 is simplified to

$$\begin{aligned} \mathbf{R}_{be} &= \underbrace{\mathbf{R}_1}_{=\mathbf{I}} \cdot \underbrace{\mathbf{Z}_{12} \cdot \mathbf{R}_2 \cdot \mathbf{Z}_{23} \cdot \mathbf{R}_3 \cdot \mathbf{Z}_{34} \cdot \mathbf{R}_4 \cdot \mathbf{Z}_{45} \cdot \mathbf{R}_5}_{=\mathbf{S}_{14}} \cdot \underbrace{\mathbf{Z}_{56} \cdot \mathbf{R}_6 \cdot \mathbf{Z}_{67} \cdot \mathbf{R}_7 \cdot \mathbf{Z}_{78} \cdot \mathbf{R}_8}_{=\mathbf{S}_{58}} \cdot \underbrace{\mathbf{I}}_{=\mathbf{I}} \quad (2) \\ &= \mathbf{I} \cdot \mathbf{S}_{14} \cdot \mathbf{R}_4 \cdot \mathbf{Z}_{45} \cdot \mathbf{R}_5 \cdot \mathbf{S}_{58} \cdot \mathbf{I} = \mathbf{S}_{14} \cdot \mathbf{R}_4 \cdot \mathbf{Z}_{45} \cdot \mathbf{R}_5 \cdot \mathbf{S}_{58}. \end{aligned}$$

Here, the simplifications  $\mathbf{R}_1 = \mathbf{I}$  and  $\mathbf{R}_8 = \mathbf{I}$  follow from the first and last row in Table 1 and the compact forms  $\mathbf{S}_{14}$  and  $\mathbf{S}_{58}$  represent the spherical subchains.

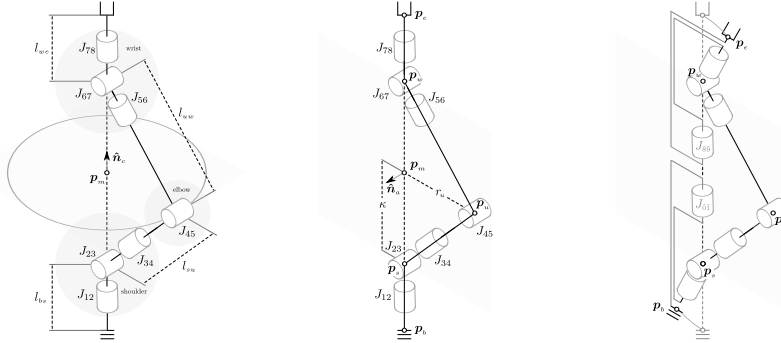
### 3 Geometry

Three planes are introduced to describe the possible postures of an SRS arm with a specific end-effector pose: the circle plane  $\mathcal{H}_c$  orthogonal to the shoulder-wrist vector  $\mathbf{d}_{sw}$  contains the current elbow position; the elbow plane  $\mathcal{H}_b$  is that affine subspace containing the positions of shoulder, elbow, and wrist; one of the elbow planes is distinguished as the reference (anchor) plane  $\mathcal{H}_a$ . See Figure 2 for three-dimensional sketches.

*Circle plane  $\mathcal{H}_c$ .* For one endeffector pose  $\mathbf{D}_{be} = \begin{pmatrix} \mathbf{R}_{be} & \mathbf{t}_{be} \\ \mathbf{0} & 1 \end{pmatrix}$ , the wrist  $\mathbf{p}_w = \mathbf{p}_s + \mathbf{d}_{sw}$  is constant since shoulder  $\mathbf{p}_s = (0, 0, l_{bs})^T$  and  $\mathbf{d}_{sw}$  are constant:

$$\begin{aligned} \mathbf{d}_{sw} &= \mathbf{p}_w - \mathbf{p}_s = (\mathbf{p}_e - \mathbf{d}_{we}) - \mathbf{d}_{bs} = (\mathbf{d}_{be} - [\mathbf{R}]_{be} \cdot [\mathbf{d}_{we}]_e) - \mathbf{d}_{bs} \\ &= \mathbf{t}_{be} - \mathbf{R}_{be} \cdot \begin{pmatrix} 0 \\ 0 \\ l_{we} \end{pmatrix} - \begin{pmatrix} 0 \\ 0 \\ l_{bs} \end{pmatrix}. \end{aligned} \quad (3)$$

Thus, a redundant arm motion only involves the elbow position. Since  $l_{su}$  and  $l_{uw}$  are constant, the elbow is constrained to a circle given as the intersection of the shoulder sphere  $\mathcal{S}_s = (\mathbf{p}_s, l_{su})$  and the wrist sphere  $\mathcal{S}_w = (\mathbf{p}_w, l_{uw})$ . The intersecting circle  $\mathcal{C}_u = \mathcal{S}_s \cap \mathcal{S}_w$  is called the circle of redundancy. The situation is indicated in Figure 2a. The normal direction  $\hat{\mathbf{n}}_c$  of the plane  $\mathcal{H}_c$  containing the redundancy circle  $\mathcal{C}_u \subset \mathcal{H}_c$  is contained is given as  $\hat{\mathbf{n}}_c = \mathbf{d}_{sw} / \|\mathbf{d}_{sw}\|$ . The circle midpoint  $\mathbf{p}_m$  is computed by solving the Pythagorean relations  $\kappa^2 + r_u^2 = l_{su}^2$  and  $(\|\mathbf{d}_{sw}\| - \kappa)^2 + r_u^2 = l_{uw}^2$  of the triangle  $\Delta = \Delta(\mathbf{p}_s, \mathbf{p}_u, \mathbf{p}_w)$  for  $\kappa = \frac{1}{2 \cdot \|\mathbf{d}_{sw}\|} \cdot (\|\mathbf{d}_{sw}\|^2 + l_{su}^2 - l_{uw}^2)$ . The center  $\mathbf{p}_m$  of the



The circle of redundancy lays in the plane  $\mathcal{H}_c$  with unit normal vector  $\hat{n}_c$  passing through the midpoint  $\mathbf{p}_m$ . Triangle geometry in the reference plane  $\mathcal{H}_a$  (or elbow plane  $\mathcal{H}_b$ ) with normal direction  $\hat{n}_a$  (or  $\hat{n}_b$ ). Illustrated virtual joints  $J_{67}$  and  $J_{55}$  for covering the redundancy circle while keeping final pose and real joints constant.

Fig. 2: Sketches of an anthropomorphic 7R arm.

redundancy circle  $\mathcal{C}_u$  is then determined as  $\mathbf{p}_m = \mathbf{p}_s + \kappa \cdot \hat{n}_c$ . Via  $\kappa$ , the radius  $r_u$  of the circle is computed with  $r_u = \sqrt{l_{su}^2 - \kappa^2}$  (see Figure 3a).

*Elbow plane  $\mathcal{H}_b$ .* In contrast to  $\Delta = \Delta(S, U, W)$  (Figure 3a), the two triangles,  $\Delta_+ = \Delta(S, U_+, W)$  and  $\Delta_- = \Delta(S, U_-, W)$ , in Figure 3b reflect the orientation of the axis of the elbow joint  $J_{45}$ . For such oriented triangles, the cyclic form of the law of cosines [2] can be applied providing the trigonometric identities

$$\begin{aligned} \cos(\gamma) &= +\cos(\alpha) \cdot \cos(\beta) - \sin(\alpha) \cdot \sin(\beta) \\ \sin(\gamma) &= -\sin(\alpha) \cdot \cos(\beta) - \cos(\alpha) \cdot \sin(\beta), \end{aligned} \quad (4)$$

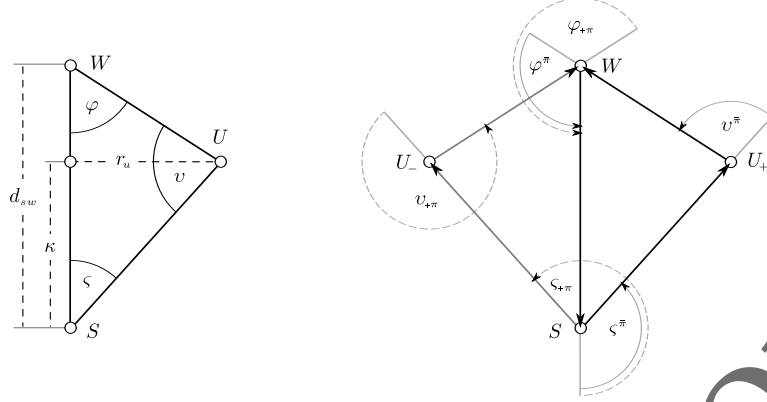
which are used to compute the oriented<sup>2</sup> angles  $v^{\pi}$  and  $v_{+\pi}$ . The solutions for elbow joint  $q_{45+}$  and  $q_{45-}$  are then derived [2] with the oriented triangles  $\Delta_+$  and  $\Delta_-$  with the compact expression

$$q_{45+}, q_{45-} = \pm \arccos(\cos(\varphi) \cdot \cos(\zeta) - \sin(\varphi) \cdot \sin(\zeta)). \quad (5)$$

The trigonometric values for  $\varphi$  are given with  $\sin(\varphi) = r_u / l_{uw}$  and  $\cos(\varphi) = (\|\mathbf{d}_{sw}\| - \kappa) / l_{uv}$  (Figure 3a). The values for  $\zeta$  are given with  $\sin(\zeta) = r_u / l_{su}$  and  $\cos(\zeta) = \kappa / \|\mathbf{d}_{sw}\|$ . Using the previously computed expressions,  $\kappa = \frac{1}{2 \cdot \|\mathbf{d}_{sw}\|} \cdot (\|\mathbf{d}_{sw}\|^2 + l_{su}^2 - l_{uw}^2)$  and  $r_u = \sqrt{l_{su}^2 - \kappa^2}$ , and simplifying the terms, the two possible elbow angles from Equation 5 are determined as<sup>3</sup>

<sup>2</sup> Given the triangle  $\Delta$  in Figure 3a with interior angles  $\zeta, v, \varphi \in [0, \pi]$ , the oriented angles of the positive-elbow triangle  $\Delta_+$  on the right hand side of Figure 3b are given as the supplementary angles  $\varphi^{\pi}, \zeta^{\pi}, v^{\pi}$  (with  $\varphi^{\pi} := \pi - \varphi$ ). The angles of the negative-elbow triangle  $\Delta_-$  on the left hand side of Figure 3b are given as the  $\pi$ -shifted angles  $\varphi_{+\pi}, \zeta_{+\pi}, v_{+\pi}$  (with  $\varphi_{+\pi} := \pi + \varphi$ ).

<sup>3</sup> In [12] only one solution is reported. Note, that the two solutions are not covered by an elbow rotation of  $\pi$ : while rotating along the circle, the elbow angle remains constant. However, the elbow configuration  $q_{45-}$  is the negative of the configuration  $q_{45+}$ : apart from any ‘stretched-out’ posture, where the two values coincide  $q_{45+} = q_{45-} = 0$ , they differ in general postures. In Figure 3b, this distinction is reflected by the counter-clockwise orientations of all six angles.



Sketch of triangle  $\Delta(S, U, W)$  spanned by shoulder  $S$ , elbow  $U$ , and wrist  $W$  with interior, undirected angles,  $\zeta$ ,  $\nu$ ,  $\varphi$ , height  $r_u$ , and edge section  $\kappa$ .

Two directed triangles  $\Delta_+ = \Delta(S, U_+, W)$  and  $\Delta_- = \Delta(S, U_-, W)$  with exterior, directed angles in counter-clockwise orientation, and directed edges directed edges  $d_{su+}$ ,  $d_{sw+}$ , and  $d_{ws+}$ .

Fig. 3: Triangles spanned by shoulder, elbow, and wrist.

$$q_{45+}, q_{45-} = \pm \arccos \left( \frac{l_{su}^2 + l_{uw}^2 - \|d_{sw}\|^2}{2 \cdot l_{su} \cdot l_{uw}} \right). \quad (6)$$

*Reference plane  $\mathcal{H}_a$ .* Each of the two triangles,  $\Delta_+$  and  $\Delta_-$ , can be rotated around the axis  $(\mathbf{p}_s, \mathbf{d}_{sw})$ . For parametrization of all points on the (two instances of the) redundancy circle, the angle  $\psi$  is defined. While the rotation axis is defined with  $\hat{\mathbf{n}}_c = \mathbf{d}_{sw}^\oplus$ , an ‘ $x$ -axis’ is not given a priori by the manipulator’s geometry. As shown in the article [12], by fixing  $q_{34}$  to zero – for a given target pose  $\mathbf{P}_e$  and a deduced elbow configuration  $q_{45}$  – values,  $q_{12}$  and  $q_{23}$ , for the first two shoulder joints,  $J_{12}$  and  $J_{23}$ , can be determined by means of using the rotative forward kinematics from Equation 2 and  $\mathbf{d}_{sw}$  from Equation 3 by solving

$$\begin{aligned} \mathbf{d}_{sw} &= \mathbf{p}_w - \mathbf{p}_s = (\mathbf{p}_s + \mathbf{d}_{su} + \mathbf{d}_{uw}) - \mathbf{p}_s = [\mathbf{R}]_{14} \cdot [\mathbf{d}_{su}]_4 + [\mathbf{R}]_{15} \cdot [\mathbf{d}_{uw}]_5 \\ &= \mathbf{S}_{14}(q_{12}, q_{23}, 0) \cdot \left( \begin{pmatrix} 0 \\ 0 \\ l_{su} \end{pmatrix} + \mathbf{R}_4 \cdot \mathbf{Z}(q_{45}) \cdot \begin{pmatrix} 0 \\ 0 \\ l_{uw} \end{pmatrix} \right). \end{aligned} \quad (7)$$

The position of the elbow joint  $\mathbf{p}_u = \mathbf{p}_s + \mathbf{d}_{su}$  for the reference angles  $q_{12}^*$  and  $q_{23}^*$ , fulfilling Equation 7, is used to define  $\psi = 0$ . According to Equation 6, two elbow positions in the elbow plane  $\mathcal{H}_b$  realize the endeffector pose. For ensuring uniqueness, the elbow position  $\mathbf{p}_{u+}$  for the positive value  $q_{45+}$  is selected to define direction of the ‘ $x$ -axis’ and the circle angle  $\psi = 0$ . The elbow plane  $\mathcal{H}_b$  is thus equipped with an interior, oriented basis by the indicator axis  $\hat{\mathbf{b}}_x = (\mathbf{p}_{u+} - \mathbf{p}_m) / \|\mathbf{p}_{u+} - \mathbf{p}_m\|$  and by the normal direction  $\hat{\mathbf{b}}_y = \hat{\mathbf{n}}_c = (\mathbf{p}_w - \mathbf{p}_s) / \|\mathbf{p}_w - \mathbf{p}_s\|$ , providing its oriented normal direction,  $\hat{\mathbf{n}}_c := \hat{\mathbf{b}}_x \times \hat{\mathbf{b}}_y$  (see Figure 2b). The reference plane  $\mathcal{H}_a$  is defined as the elbow plane  $\mathcal{H}_b$  in this specific configuration. While the orientation of  $\psi$  is induced by the normal direction of the circle plane  $\hat{\mathbf{n}}_c \cong \mathbf{d}_{sw}$ , its identity  $\psi = 0$  is fixated by the introduced reference plane  $\mathcal{H}_a$ .

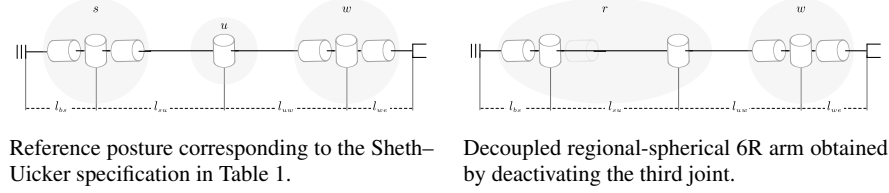


Fig. 4: Two sketches of arms in reference posture.

#### 4 Inverse Kinematics

In the first step of the inverse kinematics computation, the IKP is solved for a given endeffector pose  $\mathbf{P}_e$  with a ‘reference configuration’ for the joints. In the second step, the modifications of this configuration for (i) swapping to a different instances of the circle and (ii) letting the elbow travel along the redundancy circle are outlined. *First Step.* A feasible elbow angle  $q_{45}^*$  can be selected from Equation 6. A feasible reference configuration for  $q_{12}^*, q_{23}^*, q_{34}^*$  is determined with Equation 7. For such selected four angles  $q_{12}^*, q_{23}^*, q_{34}^*, q_{45}^*$ , a configuration for the joints of the spherical shoulder,  $J_{56}, J_{67}, J_{78}$ , can be computed by solving Equation 2 for

$$\mathbf{S}_{58}(q_{56}, q_{67}, q_{78}) = \underline{\mathbf{R}}_5^T \cdot \mathbf{Z}^T(q_{45}^*) \cdot \underline{\mathbf{R}}_4^T \cdot \mathbf{S}_{14}^T(q_{12}^*, q_{23}^*, q_{34}^*) \cdot \mathbf{R}_{ie}. \quad (8)$$

In total, one feasible solution  $\mathbf{q}^* = (q_{12}^*, q_{23}^*, q_{34}^*, q_{45}^*, q_{56}^*, q_{67}^*, q_{78}^*)^T$  to the Inverse Kinematics Problem is obtained.

*Second Step.* Given a feasible configuration  $\mathbf{q}^*$  selected in the first step, the second step consists of modifying this configuration in such way that the elbow travels along (one of the eight instances of) the redundancy circle. The selected reference configuration  $\mathbf{q}^*$  fulfills the forward kinematics Equation 1, and in particular, the rotative pendant  $\mathbf{R}_{be} = \mathbf{S}_{14}^* \cdot \underline{\mathbf{R}}_4 \cdot \mathbf{Z}_{45}^* \cdot \underline{\mathbf{R}}_5 \cdot \mathbf{S}_{58}^*$ , Equation 2, with the shoulder matrix  $\mathbf{S}_{14}^* = \mathbf{S}_{14}^*(q_{12}^*, q_{23}^*, q_{34}^*) = \mathbf{Z}(q_{12}^*) \cdot \underline{\mathbf{R}}_2 \cdot \mathbf{Z}(q_{23}^*) \cdot \underline{\mathbf{R}}_3 \cdot \mathbf{Z}(q_{34}^*)$ , the elbow matrix  $\mathbf{Z}_{45}^* = \mathbf{Z}(q_{45}^*)$ , and the wrist matrix  $\mathbf{S}_{58}^* = \mathbf{S}_{58}^*(q_{56}^*, q_{67}^*, q_{78}^*) = \mathbf{Z}(q_{56}^*) \cdot \underline{\mathbf{R}}_2 \cdot \mathbf{Z}(q_{67}^*) \cdot \underline{\mathbf{R}}_3 \cdot \mathbf{Z}(q_{78}^*)$ . The change of the elbow position on the redundancy circle is expressed by introducing the virtual joints  $J_{01}$  and  $J_{89}$  into the chain (Figure 2c) as

$$\mathbf{R}_{be} = \underline{\mathbf{R}}_0 \cdot \mathbf{Z}_{01}(\psi) \cdot \underline{\mathbf{R}}_1 \cdot \mathbf{S}_{14}^* \cdot \underline{\mathbf{R}}_4 \cdot \mathbf{Z}_{45}^* \cdot \underline{\mathbf{R}}_5 \cdot \mathbf{S}_{58}^* \cdot \underline{\mathbf{R}}_8 \cdot \mathbf{Z}_{89}(-\psi) \cdot \underline{\mathbf{R}}_9.$$

Here,  $\underline{\mathbf{R}}_0$  maps the  $z$ -axis of the base frame to the direction  $\hat{\mathbf{n}}_c$ , and  $\underline{\mathbf{R}}_1$  describes the inverse rotation  $\underline{\mathbf{R}}_1 = \underline{\mathbf{R}}_0^T$ . Similarly,  $\underline{\mathbf{R}}_8$  maps the  $z$ -axis of the endeffector frame to the direction  $\hat{\mathbf{n}}_c$ , and  $\underline{\mathbf{R}}_9$  describes the inverse rotation  $\underline{\mathbf{R}}_9 = \underline{\mathbf{R}}_8^T$  (Figure 2c).

A configuration  $\mathbf{q}$  that realizes a certain redundancy angle  $\psi$  is computed by ‘pushing’ the displacement of the two virtual joints into the joint configuration  $\mathbf{q}^*$ . A shoulder configuration  $(q_{12}, q_{23}, q_{34})$  is computed so that the wrist displacement  $\mathbf{S}_{14} = \mathbf{S}_{14}(q_{12}, q_{23}, q_{34})$  compensates for the rotation  $\mathbf{Z}_{01}(\psi)$  of the virtual joint  $J_{01}$  as

$$\mathbf{S}_{14} = \underline{\mathbf{R}}_0 \cdot \mathbf{Z}_{01}(\psi) \cdot \underline{\mathbf{R}}_1 \cdot \mathbf{S}_{14}^* = \exp(\psi \cdot \hat{\mathbf{n}}_c^\otimes) \cdot \mathbf{S}_{14}^* \quad (9)$$

with  $\mathbf{a}^\otimes := \begin{pmatrix} 0 & -a_3 & a_2 \\ a_3 & 0 & -a_1 \\ -a_2 & a_1 & 0 \end{pmatrix}$ . For the wrist, a spherical displacement  $\mathbf{S}_{58} = \mathbf{S}_{58}(q_{56}, q_{67}, q_{78})$  compensating for the rotation  $\mathbf{Z}_{89}(-\psi)$  of the virtual joint  $J_{89}$  is computed with

**Algorithm 1** Euler angle computation (ZYZ-convention)

(in) Rotation matrix $\mathbf{R} = \mathbf{R}_z(\gamma) \cdot \mathbf{R}_y(\beta) \cdot \mathbf{R}_z(\alpha)$	7:	$\gamma_+ \leftarrow \text{atan}_2(+\mathbf{R}_{[2,3]}, +\mathbf{R}_{[1,3]}/s)$
(out) Euler angles $(\gamma_+, \beta_+, \alpha_+), (\gamma_-, \beta_-, \alpha_-)$	8:	$\gamma_- \leftarrow \text{atan}_2(-\mathbf{R}_{[2,3]}, -\mathbf{R}_{[1,3]}/s)$
1: <b>function</b> ROTMAT-2-EA-ZYZ( $\mathbf{R}$ )	9:	<b>else</b> <span style="float: right;"># Singular</span>
2: $\beta_+ \leftarrow \text{acos}(\mathbf{R}_{[3,3]}), \beta_- \leftarrow -\beta_+$	10:	$\alpha_+ \leftarrow \text{atan}_2(\mathbf{R}_{[1,2]}, \mathbf{R}_{[1,1]})$
3: $s \leftarrow \sin(\beta_+)$	11:	$\alpha_- \leftarrow 0$
4: <b>if</b> $s \neq 0$ <b>then</b> <span style="float: right;"># Regular</span>	12:	$\gamma_+ \leftarrow 0$
5: $\alpha_+ \leftarrow \text{atan}_2(+\mathbf{R}_{[3,2]}/s, -\mathbf{R}_{[3,1]}/s)$	13:	$\gamma_- \leftarrow \text{atan}_2(\mathbf{R}_{[1,2]}, \mathbf{R}_{[1,1]})$
6: $\alpha_- \leftarrow \text{atan}_2(-\mathbf{R}_{[3,2]}/s, +\mathbf{R}_{[3,1]}/s)$	14:	<b>return</b> $(\gamma_+, \beta_+, \alpha_+), (\gamma_-, \beta_-, \alpha_-)$

Table 2: Matrix-to-zyz-angle conversion method

$$\begin{aligned} \mathbf{S}_{58} &= \mathbf{S}_{58}^* \cdot \underline{\mathbf{R}}_8 \cdot \mathbf{Z}_{86}(-\psi) \cdot \underline{\mathbf{R}}_9 = \mathbf{S}_{58}^* \cdot [\mathbf{R}]_{eb} \cdot \exp(-\psi \cdot \hat{\mathbf{n}}_c^\otimes) \cdot [\mathbf{R}]_{be} \\ &= \mathbf{S}_{58}^* \cdot [\exp(-\psi \cdot \hat{\mathbf{n}}_c^\otimes)]_{ee}. \end{aligned} \quad (10)$$

For augmenting the computation with the second solution,<sup>4</sup> the modeling via Sheth–Uicker parameters (Table 1) offers a straightforward approach: The link displacement rotations  $\underline{\mathbf{R}}_2, \underline{\mathbf{R}}_3, \underline{\mathbf{R}}_6,$  and  $\underline{\mathbf{R}}_7$ , defined by  $\beta_2, \beta_3$  and  $\beta_6, \beta_7$  from Table 1, are quarter-turn matrices with coordinates

$$\underline{\mathbf{R}}_2 = \underline{\mathbf{R}}_6 = \mathbf{R}_x(-\frac{\pi}{2}) = \begin{pmatrix} 1 & 0 & 0 \\ 0 & 0 & +1 \\ 0 & -1 & 0 \end{pmatrix} \quad \underline{\mathbf{R}}_3 = \underline{\mathbf{R}}_7 = \mathbf{R}_x(+\frac{\pi}{2}) = \begin{pmatrix} 1 & 0 & 0 \\ 0 & 0 & -1 \\ 0 & +1 & 0 \end{pmatrix}.$$

With these properties and  $\mathbf{R}_x(-\pi/2) \cdot \mathbf{R}_x(+\pi/2) = \mathbf{I}$ , it is observed that the shoulder displacement  $\mathbf{S}_{14} = \mathbf{Z}(q_{12}) \cdot \underline{\mathbf{R}}_2 \cdot \mathbf{Z}(q_{23}) \cdot \underline{\mathbf{R}}_3 \cdot \mathbf{Z}(q_{34})$  and the wrist displacement  $\mathbf{S}_{58} = \mathbf{Z}(q_{56}) \cdot \underline{\mathbf{R}}_6 \cdot \mathbf{Z}(q_{67}) \cdot \underline{\mathbf{R}}_7 \cdot \mathbf{Z}(q_{78})$  feature the shape of an Euler rotation matrix in ZYZ-convention. For this reason, the joint configurations for the matrices  $\mathbf{S}_{14}$  and  $\mathbf{S}_{58}$ ,

$$\mathbf{S}_{14} = \exp(\psi \cdot \hat{\mathbf{n}}_c^\otimes) \cdot \mathbf{S}_{14}^* \quad \mathbf{S}_{58} = \mathbf{S}_{58}^* \cdot [\exp(-\psi \cdot \hat{\mathbf{n}}_c^\otimes)]_{ee}, \quad (11)$$

from Eq. 9 and Eq. 10 can be computed with Alg. 2. Since the conversion method returns two solution for the shoulder triplet  $(q_{12}, q_{23}, q_{34})$  and for the wrist triplet  $(q_{56}, q_{67}, q_{78})$ , and considering the two solutions for the elbow joint  $q_{45}$  (Eq. 6), the size of the solution space (for a nonsingular configuration) is determined as

$$|\text{CONFIGS}| = |\text{SHOULDER}| \cdot |\text{ELBOW}| \cdot |\text{WRIST}| \cdot |\text{CIRCLE}| = 2 \cdot 2 \cdot 2 \cdot (\infty^1) = 8 \cdot (\infty^1)$$

coherent to eight IKP solutions of a corresponding regional-spherical arm (Fig. 4b). *Example.* An example for solutions to the inverse kinematics problem on eight different circles is shown in Figure 5. The signum triplets in the captions indicate the flips of the subchains shoulder, elbow, and wrist.

<sup>4</sup>For determining the shoulder angles and wrist angles from the matrices  $\mathbf{S}_{14}$  and  $\mathbf{S}_{58}$ , the method in [12] is based on orthogonal decomposition of rotation matrices and solving for  $(q_{12}, q_{23}, q_{34})$  and  $(q_{56}, q_{67}, q_{78})$ , by coefficient comparison with respect to  $\psi$ . For the shoulder, the equation

$$\mathbf{S}_{14}(q_{12}, q_{23}, q_{34}) = \exp(\psi \cdot \hat{\mathbf{n}}_c^\otimes) \cdot \mathbf{S}_{14}^* = \sin(\psi) \cdot \underbrace{\hat{\mathbf{n}}_c^\otimes \cdot \mathbf{S}_{14}^*}_{=: \mathbf{A}_s} + \cos(\psi) \cdot \underbrace{(-\hat{\mathbf{n}}_c^\otimes)^2 \cdot \mathbf{S}_{14}^*}_{=: \mathbf{B}_s} + \underbrace{\hat{\mathbf{n}}_c^\otimes \cdot \mathbf{S}_{14}^*}_{=: \mathbf{C}_s},$$

with  $\mathbf{a}^\otimes := \mathbf{a} \cdot \mathbf{a}^T$ , and the coefficients of  $\mathbf{S}$  are analyzed. For the wrist, a similar approach is chosen. In both cases, the coefficient analysis only reports one of the two feasible solutions.

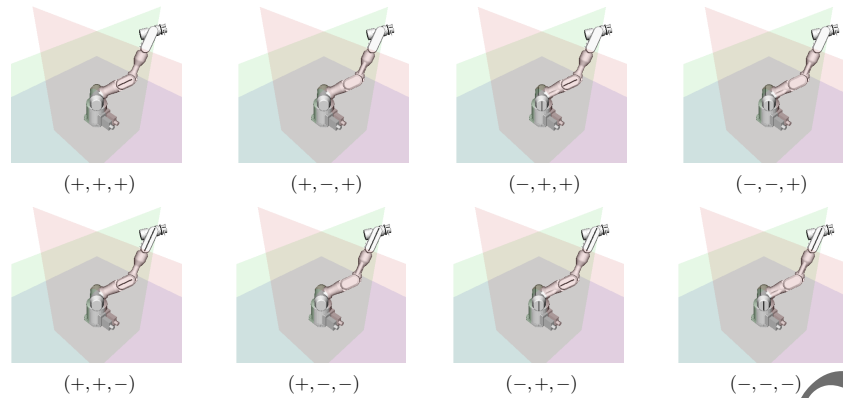


Fig. 5: Example of eight different joint configurations corresponding one endeffector pose and one elbow position. The links of the robot are marked with black lines to distinguish the postures.

## 5 Conclusion and Outlook

The paper documents eight coinciding circles with  $8 \cdot (\infty^1)$  solutions for the inverse kinematics problem of anthropomorphic arms and provides an essential step for using all capabilities of such manipulators. For this goal, the interval analysis [12] can be combined with the presented modeling and computation in the future.

**Acknowledgements** The work was performed within the projects *Capio* and *Recupera*, funded with federal funds from the German Federal Ministry of Education and Research (BMBF) (Grant 01-IW-10001 and 01-IM-14006A). The author would like to thank Sankaranarayanan Natarajan, Wiebke Drop, and Arnaud Sengers for their contributions.

## References

- [1] T. Asfour and R. Dillmann. "Human-like motion of a humanoid robot arm based on a closed-form solution of the inverse kinematics problem". In: *Int. Conference on Intelligent Robots and Systems (IROS)*. 2003.
- [2] B. Bongardt. "Analytic Approaches for Design and Operation of Haptic Human-Machine Interfaces". PhD thesis. Universität Bremen, 2015.
- [3] B. Bongardt. "New Solutions for the Null-Space of Anthropomorphic 7R Arms (Extended Abstract)". In: *IFTOMM D-A-CH*. Feb. 2016.
- [4] B. Bongardt. "Sheth-Uicker convention revisited". In: *Mechanism and Machine Theory* 69 (2013).
- [5] J. W. Burdick. "On the inverse kinematics of redundant manipulators: characterization of the self-motion manifolds". In: *Int. Conf. on Robotics and Automation (ICRA)*. 1989.
- [6] P. Dahm and F. Joublin. *Closed form solution for the inverse kinematics of a redundant robot arm*. Technical report. IRINI 97-08, 1997.
- [7] A. Dietrich, C. Ott, and A. Albu-Schäffer. "An Overview of Null Space Projections for Redundant, Torque-Controlled Robots". In: *Int. Journal of Robotics Research* (2015).
- [8] R. S. Hartenberg and J. Denavit. "A kinematic notation for lower-pair mechanisms based on matrices". In: *Journal of Applied Mechanics* 22 (1955).
- [9] J. M. Hollerbach. "Optimum kinematic design for a seven degree of freedom manipulator". In: *Int. Symposium on Robotics Research*. 1985.
- [10] M. Pfurner. "Closed Form Inverse Kinematics Solution for a Redundant Anthropomorphic Robot Arm". In: *Computer Aided Geometric Design* 47 (2016).
- [11] P. N. Sheth and J. J. Uicker. "A Generalized Symbolic Notation for Mechanisms". In: *Journal of Engineering for Industry, Series B* 93.70 (1971).
- [12] M. Shimizu, H. Kakuya, W.-K. Yoon, K. Kitagaki, and K. Kosuge. "Analytical Inverse Kinematic Computation for 7-DOF Redundant Manipulators With Joint Limits and Its Application to Redundancy Resolution". In: *IEEE Transactions on Robotics* 24 (2008).